

CFD modeling of turbulent boundary layer flow in passive drag-reducing applications

R. I. Bourisli¹ & A. A. Al-Sahhaf²

¹*Department of Mechanical Engineering, Kuwait University, Kuwait*

²*School of Engineering and Design, Brunel University, UK*

Abstract

In this paper, the turbulence boundary layer, velocity and skin friction coefficient characteristics of grooved surfaces are studied. Flow over surfaces with transverse square, triangular and semicircular grooves are numerically modeled via the finite volume method. Comparisons are made on the basis of the grooved surfaces' skin-friction coefficient, normalized by that of a smooth surface, with Reynolds number in the vicinity of 2×10^6 . Results show that square grooves are superior to the two other groove geometries in reducing the drag. Viscous damping in all grooves keeps skin friction inside them well below the surface above. However, the interior geometry of square grooves allows them to balance the net inward momentum due to the sudden absence of the wall in a way that minimizes disturbance of the main flow while taking advantage of the restart of the boundary layer. As a consequence to the separation of the boundary layer, an inevitable stagnation point within the groove must exist. Square grooves had the highest such stagnation point along the backward-facing side of the groove. The shortness of the resulting upward boundary layer from the stagnation point to the corner produces smaller near-wall secondary flow motion and more relaxed merger with the main flow. All this contributes to enhanced drag reduction for the described groove structure.

Keywords: viscous drag, skin-friction coefficient, grooved surfaces, turbulent boundary layer, momentum transfer.

1 Introduction

In the past, turbulence was thought to be totally random in terms of its microscopic flow behavior and initiation mechanisms. However, some sort of order was found in turbulent flows (Hama et al. [1] and Kline et al. [2]) which allowed engi-



neers to begin work on trying to control them. The problem of reducing drag for external flows over surfaces is one such endeavor; it has been the subject of much research, off and on, for the past few decades. The basic methodology has been to delay laminar-to-turbulence transition, with the primary intention of reducing skin-friction drag. With recent energy and environmental concerns, improvement of the efficiency of transportation means has seen a renewed focus. The subject is relevant to a large number of areas as it relates to more than a few devices across many engineering applications, each with direct influence on energy consumption. For example, in civil or commercial transport aircraft, viscous or skin friction drag is responsible for about 40–50% of the total drag under typical cruise conditions [3]. Therefore, enhancing the drag-related hydrodynamic performance of these curved surfaces can lead directly to huge increase in fuel efficiency, even if the reductions are small. Since most of these vessels operate in the turbulent regime, understanding turbulent flow behavior at the surfaces and how it relates to the possibility of drag reduction becomes extremely important.

Various techniques have been proposed over the years with the aim of reducing the drag experienced by solid bodies moving in viscous fluids. Passive techniques have generally been concerned with using surface grooves and micro-grooves (riblets) to alter near-wall turbulence in a way that reduces wall shear stress. The suggestion that drag can be reduced using transverse square grooves was originally suggested by Tani et al. [4]. The plethora of subsequent heavily-investigated techniques included longitudinal (streamwise) and transverse grooves, with the shape of grooves frequently being square or triangular, with round and rectangular getting less attention.

However, it was discovered early that turbulent flow regime greatly influences the effectiveness of such techniques. Ching and Parsons [5] studied the drag characteristics of the turbulent boundary layer over flat plates with transverse square grooves using direct drag measurements in a tow tank. They reported little to no reduction in total drag for the cases tested. In fact, many of the configurations tested resulted in drag increase on the order of 1%. The large number of variables and flow settings involved gave rise to a large body of research in this area that is continually growing.

Viswanath [3] thoroughly reviewed the performance of the longitudinally-applied 3M riblets on airfoils, wings and wing-body configurations at different speed regimes. He reported drag reductions of 5–8% for airfoils and 2–3% for wing-body configurations. He also reported that riblets are more effective in adverse pressure gradients. Caram and Ahmed [6] also studied the near and intermediate wake region of the NACA 0012 airfoil and reported drag reduction as high as 13%, the non-monotonic variation of drag reduction with riblet height raised some doubts regarding measurements accuracy.

Use of compliant coating to reduce drag was first proposed by Kramer [7]. He observed that stability and transition characteristics of a boundary layer can be modified by hydroelastic-coupling to compliant coating. Various subsequent research in that field has met varying degree of success. Gad-el-Hak [8] provided an excellent review of progress in this field.



Kato et al. [9] presented a theoretical analysis of potential heat transfer enhancement and the associated pressure loss as they relate to the roughness in turbulent channel flows. The use of roughness elements is a typical example of utilizing turbulence to increase heat transfer coefficient. They analytically confirm, however, that the enhancement in heat transfer is usually accompanied by an increase in drag, contrary to original desires. They also noted that, given the definition of Prandtl number as the ratio of effective diffusivity to heat transfer, the momentum transfer will always be more effective when the Prandtl number is less than or equal to the turbulent Prandtl number.

Another thermally-related drag question is whether varying the thermal gradient between the surface and fluid modify the surface shear stress distribution and the resulting skin-friction drag. Polidori et al. [10] investigated the effect in the context of underwater swimming. They tried to theoretically quantify the effect the integral formalism applied to the forced convection theory. It was demonstrated that, regardless of the flow Reynolds number, a 5% reduction in the skin-friction drag would occur by increasing average *laminar* boundary-layer temperature. For a turbulent flow analysis, which is more relevant to practical applications, the effect was less pronounced, with at most 1.5% reduction for medium to high Reynolds numbers. The authors correctly conclude that for turbulent flows the skin-friction drag is solely a function of Reynolds numbers.

While passive techniques are simple, easy to apply, and inexpensive, more recently, active feedback control with distributed micro sensors and actuators were the subject of much attention. The potential large modification of boundary layers and of the overall flow field with the small controlled input made such active devices attractive wherever their installation is feasible. In some Reynolds numbers ranges, drag reduction as high as 20% can be established, albeit after some time has elapsed, as reported by Endo et al. [11]. Despite their robustness in hostile environments and little fouling potential, however, complex construction, complex method of attachment, and difficulty of attachment to existing surfaces make their use less attractive. The high initial cost, the auxiliary power required to actuate the wall, and the extra space needed to host the hardware constitute additional constraints.

The two main variables to consider in such configurations are the groove spacing (s) and width (w). In general, a reduction in the wall shear stress (τ_w) is observed at the start of the groove where the boundary layer separates. The sudden temporary absence of the wall weakens the streamwise vorticity promoting the observed response by the near-wall flow. The observed drop in τ_w is followed by a sharp rise immediate downstream of the groove. The sharp rise in τ_w is commonly attributed to the local intense favorable pressure gradient emanating from the downstream edge of the groove. Research on exactly how the geometry of the grooves influence the flow dynamics and turbulent boundary layer structure is seldom found. This will be the primary focus of the current study.

This paper tries to address the following basic questions: 1) is the shape of the groove a factor in the amount of skin drag reduction? and if so, to what degree? 2) How does the shape of the groove influence the structure of the tur-



bulent boundary layer and flow outside the groove? Lastly, 3) what effect do modeling techniques have on any reported results? Some observations are also made on to what degree the performance of one groove strategy changes across ranges of Reynolds number. The first question determines the required type and range of surface treatments, while the second provides some insight on how future groove geometry modification might be geared toward enhancing drag reduction capabilities. The third question provides some guidelines regarding proper ways to model this effect for future applications and designs, at least in the Reynolds number range addressed. The observations made with regards to this last point will help specify the type of treatment most effective for multi-Reynolds number applications. To do this, the paper is organized as follows. Section 2 gives the formulation of the problem in terms of geometry, governing equations, and appropriate models used. Section 3 lists the results of the numerical simulations and discusses them from a physical as well as numerical point of view. Section 4 draws conclusions from the work presented and summarizes lessons learned for future use in similar simulations.

2 Formulation and numerical method

2.1 Geometry and governing equations

To give the problem practical dimensions, all the cases considered were modeled using a 2-D flat plate with a total length of 3 m, with treatment limited to the middle 1 m only. The physical structure can be encountered in numerous real-world applications, such as automobiles, ship hulls, aircraft wings, etc. The freestream velocity chosen for cases reported was 33 m/s which corresponding to a Reynolds number of 2×10^6 based on a characteristic length $L_c = 1$ m. The Reynolds number based on momentum thickness, Re_θ , is 4000 at the start of the grooved section. These values were specifically chosen to facilitate the necessary validation with the experimental data for a comparably grooved flat plate with square grooves done by Wahidi et al. [12].

Tested grooves were square, triangular and semicircular in shape. Various widths and depths were tested and comparison is presented for 2 mm wide, 2 mm deep grooves (1 mm radii semicircular) that are 20 mm apart. Comparisons are made between grooved middle sections and a comparable (middle 1 m) smooth section of the plate. Initial studies show that any pertinent effects of slight curvature can be neglected for purposes of this study. Deviation from true 3-D behavior is addressed in Section 4. The flow is governed by the steady, incompressible, Reynolds-averaged Navier-Stokes equations, shown below in dimensionless, primitive variable form,

$$\nabla \cdot u = 0 \quad (1)$$

$$(u \cdot \nabla)u = -\nabla p + \frac{1}{Re} \nabla^2 u \quad (2)$$



The k - ϵ model set of equations for eddy viscosity, turbulent kinetic energy, dissipation rate and closure coefficients can be found in any basic text on turbulence (see [13] for example). Double precision is used for all variables and a freestream velocity of 33 m/s and air were chosen as a base case.

Standard velocity inlet boundary condition was used for the inlet and standard pressure outlet was used for the exit. The plates were assumed stationary with a dimensionless roughness height of $k_s^+ = 0.5$. The boundary condition for the outer part of the flow for the rectangular domain is an important issue. The specification of the realistic pressure-far-field boundary condition is incompatible with the incompressibility assumption. Therefore, the symmetry boundary condition was specified at the top of the modeled region. This usually alters the physics of the flow because the presence of a solid surface is assumed at twice the height of the modeled region. To get around this artifact, the displacement thickness is precalculated using a generic $1/7$ power law turbulent profile, $\delta^* = 0.046xRe_x^{-1/5}$, and the inlet velocity was corrected accordingly to give the desired Re and Re_θ values at the start of the grooved section.

2.2 Boundary layer resolution

The presence of solid surfaces greatly affects the behavior of turbulent flows, both in terms of velocity as well as turbulence variables. The solid surface is where the gradients are the largest, and, more importantly, it is where the flow turbulence kinetic energy and vorticity are produced. These vigorous fluctuations in momentum and other scalar transport variables have to be resolved accurately in order to have a faithful description of the secondary variables of interest. The turbulence model of choice (the k - ϵ model) is known to be primarily valid for turbulent core flow, away from solid surfaces. To ensure accurate prediction of variables throughout the boundary layer, particularly in the near-wall region, mesh resolution must be fine enough, but not finer.

In addition, the RNG (renormalization group theory) version of the standard k - ϵ turbulence model was used for this study. This model is similar to the standard model but includes an additional term that improves accuracy for rapidly strained flows.¹ While computationally more demanding, the convergence rate and solution quality of the RNG model justifies its use in such and similar flow simulations.

Numerous experiments have shown that turbulent boundary layers can largely be subdivided into three layers: the viscous sublayer, the log layer and the defect layer. Turbulence models are usually modified to enable the boundary to be resolved with a fine mesh from the outer edge of the boundary layer all the way to the wall, including the viscous sublayer. This approach was followed here for accurate prediction of wall shear stress, frictional drag, pressure drop, turbulence variables, and similar variables of interest. The complete resolution of the turbulent boundary layer usually imposes considerable computational load on the

¹The RNG model also includes the effect of swirl on turbulence and an analytical formula for Pr_t which further enhances its accuracy.



solution algorithm. One would want to have a boundary layer formulation that is fine enough to resolve the turbulent sublayers, particularly the (laminar) viscous sublayer, and, at the same time, be coarse enough to facilitate realistic modeling turnaround times. To accomplish this goal, FluentTM two-layer model with enhanced wall functions is used [14].

To non-dimensionalize the velocity profile in the turbulent boundary layer, we use the dimensionless velocity, u^+ , and distance, y^+ , defined as,

$$u^+ \equiv \frac{\bar{u}}{u_\tau}, \quad (3)$$

$$\text{and } y^+ \equiv \frac{u_\tau y}{\nu} \quad (4)$$

where $u_\tau \equiv \sqrt{\tau_w/\rho}$ is the friction velocity, τ_w is the shear stress at the surface, ρ is the density, and ν is the kinematic viscosity. As with the laminar boundary layer, close to the surface, the horizontal velocity varies linearly with distance, equation (5). For $y^+ \geq 7$ the velocity gradually asymptotes to the well-known *law of the wall*, obeying equation 6 between $y^+ = 30$ and $y = 0.1\delta$, where δ is the total boundary layer thickness. Further away from the surface, the velocity profile makes a noticeable departure from the law of the wall. A correlation of measurements, equation (7), combines the velocity behavior in the log and defect layers incorporating the Coles' wake-strength parameter, $\tilde{\Pi} \approx 0.6$.

$$u^+ = y^+ \quad \text{viscous sublayer} \quad (5)$$

$$u^+ = \frac{1}{\kappa} \ln y^+ + 5 \quad \text{log layer} \quad (6)$$

$$u^+ = \frac{1}{\kappa} \ln y^+ + 5 + \frac{2\tilde{\Pi}}{\kappa} \sin^2\left(\frac{\pi y}{2\delta}\right) \quad \text{log + defect layers} \quad (7)$$

An effective accuracy test for the mesh suitability of any turbulent flow simulation is the reproduction of the three sublayers of the turbulent boundary layer. A base case representing a smooth plate was constructed, meshed, remeshed, and tweaked (mainly using the *Adapt* feature of Fluent for better targeted refinement) until a satisfactory mesh resolution is reached with respect to the experimentally-verified boundary layer relations above. Specifically, boundary layer mesh adaption was done based on the combined consideration of three quantities: grid iso-value, parallel velocity gradient, and y^+ iso-value. The bottom-right mesh of figures 1 shows a sample resultant adaption effect for part of the flat surface. The initial tuning of the boundary layer mesh produced the excellent agreement shown in figure 2. For subsequent (grooved) cases, only the small, comparably-meshed grooves (with different sizes and shapes) were added and attached to the flow domain. Similar adaption was also performed once the final grooved surface geometry is being solved. The top two and the bottom-left meshes of figure 1 show sample resultant adaption effects for the three types of grooves.



3 Results and discussion

3.1 Skin friction coefficient

Initial comparisons between grooves geometry are done by straightforward integration of the skin friction coefficient over the whole middle section of surfaces

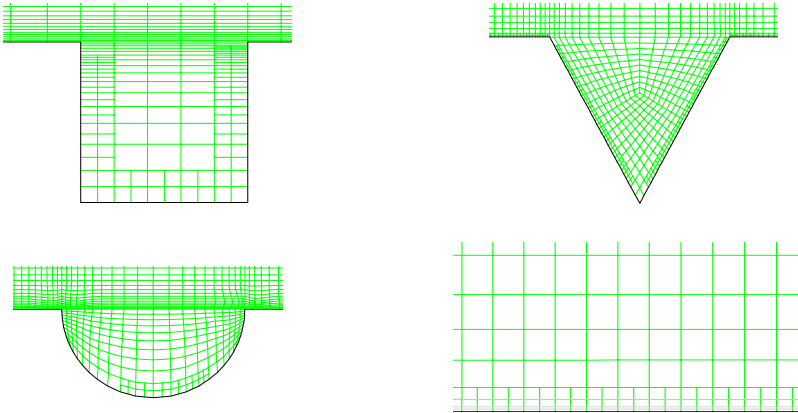


Figure 1: Adaption results for the geometry based on the combined consideration of velocity gradients, and grid and y^+ iso-values.

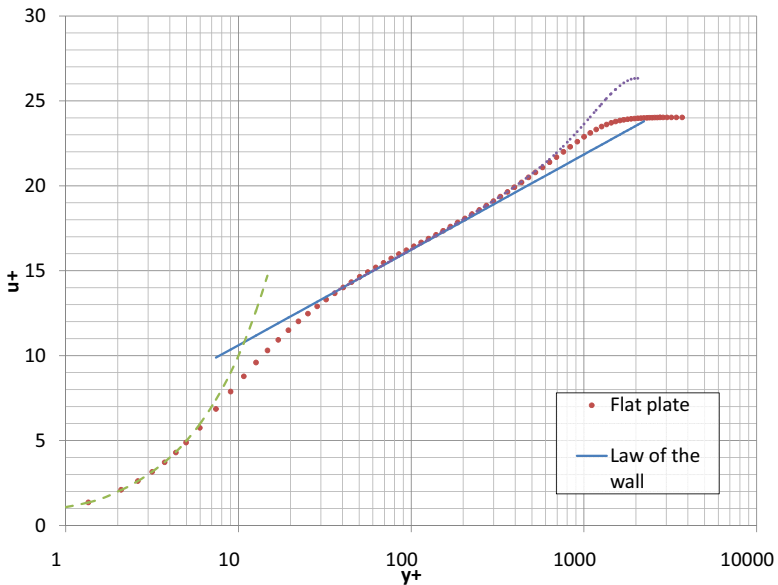


Figure 2: Velocity profile for the turbulent boundary layer flow compared experimental correlation.



including any horizontal components of interior groove surfaces. These comparisons clearly favor the square and semicircular grooves over the triangular ones. For the specified geometry and boundary conditions, reductions in skin friction were 8% for square grooves and 7.6% for semicircular ones. Triangular grooves provided little or no reduction at all. In fact, for the best square case, substituting triangular grooves resulted in a 3.6% drag increase. This finding is intriguing if one notices that triangle are far superior to other shapes when the grooves are placed longitudinally [3]. This point will be addressed when the dynamics of the flow inside the grooves are discussed further below.

One primary mechanism by which grooved surfaces are believed to reduce friction drag is delaying transition. One way of accomplishing a similar effect that is pertinent to the current type of treatment is “restarting” the boundary layer at a proper place in a way that takes advantage of the sudden drop in shear stress due to the sudden absence of the wall but does not let it grow thick enough to wipe out any benefit scored. The flow generally exhibits a drop in friction coefficient over the groove and a spike at the restart of the boundary layer over the next section downstream. The general picture and numbers compare well with experimental results reported by Wahidi [12].

Figure 4 shows the skin friction coefficient, normalized by the skin friction value of the same location for a smooth surface, upstream of, over and downstream of a typical (middle) groove. The dots are connected via simple smoothed lines for ease of viewing. Taking the grooves one by one, one can make the following obvious observations regarding the behavior of the friction coefficient. First, for the square groove, the friction coefficient drops suddenly over the groove, builds up gradually along the bottom of the groove, and then peaks slightly at the restart of the surface. The increase and decrease in friction is smooth and monotonic, with no kinks, mainly because of the simple geometry of the square groove. Additionally, one notices that upstream and downstream of the groove, the skin friction is not the lowest. This is a result of the gradual built-up modification of the boundary layer by grooves upstream of the groove shown. Finally, we see that the peak of the friction coefficient at the restart of the boundary layer is not very sharp. This is addressed further when the momentum of the flow is discussed in the next subsection for this and the two other groove geometry.

For the triangular groove, skin friction peaks just before the groove, drops suddenly, then fluctuates around the sharp bottom of the groove. It makes a noticeable jump before the level flat surface is reached, and spikes considerably at the restart of the boundary layer. We notice that despite the fluctuations, the triangular groove has the lowest friction coefficient inside the actual groove. The cumulative effect of such spikes, however, are seen in the higher than average skin friction far away from the triangular groove, explaining their poor performance as mentioned above.

Finally, for the semicircular groove, which has the lowest upstream and downstream skin friction levels, the behavior is relatively simpler. After the initial drop, the skin friction monotonically increases over the semicircular surface of the groove then quickly drops at separation and spikes again at the beginning of the boundary layer downstream of the groove. The skin friction values as well as the



spike at separation are comparable to the square groove's, which explains the close performance of these two geometries in the overall calculation of the skin friction presented in figure 4.

3.2 Cross-flow momentum transfer

To understand the mechanism of the turbulent flow in and around the flow and how the geometry might affect the separation and restart of the boundary layer, one must consider the interaction between the main flow and any small-scale flow emanating from the grooves. Figures 3 show velocity vector plots in and around the typical square, triangular and semicircular grooves. In general, turbulence rarely penetrates into the grooves, making the shear stress and thus skin friction much lower than that over the flat part of the surface. Moreover, inside the grooves, the large viscous damping reduces the tangential fluctuations in velocity, while kinematic blocking reduces the normal fluctuations. However, the dynamic behavior of the flow inside the grooves greatly affects their compound effect on the overall reduction or increase in drag over the whole surface.

Pound-for-pound, square transverse grooves are expected to induce lower shear stress in the direction of the flow than, say, triangular grooves, for two reasons: first, the vertical walls do not contribute directly to the surface shear stress parallel to the main flow direction. Secondly, the bottom walls of the grooves are well below the main flow in a way that deems the resultant friction much lower due to decreased velocity inside the grooves. Semicircular grooves, on the other hand, have smooth interiors but are relatively closer to the main flow than are the other two groove shapes. Detailed discussion of velocity vectors is presented below.

The symmetric, sharp geometry of the square groove sustains enough equilibrating pressure for the flow just above the groove so as to keep the disturbance of the main flow to a minimum after separation has taken place. The high point of reattachment on the opposite wall of the groove allows the boundary layer to make

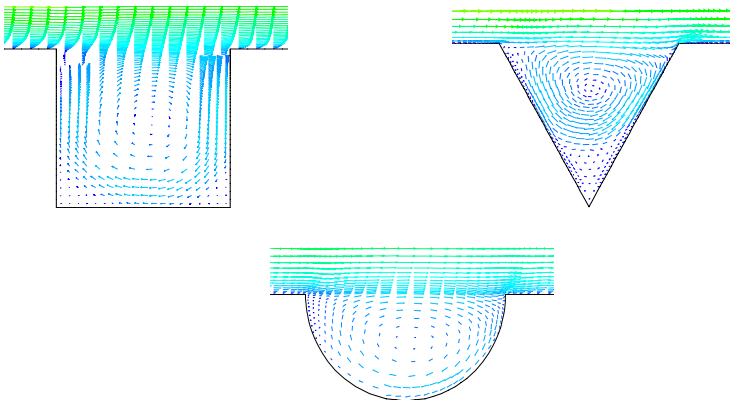


Figure 3: Velocity vectors in and around grooves.



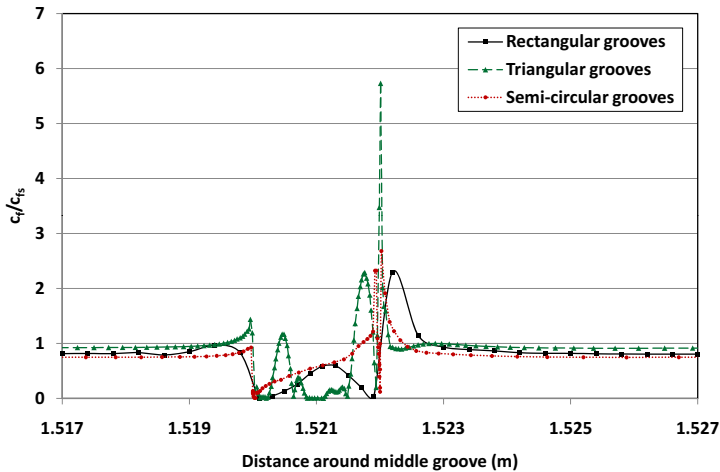


Figure 4: Normalized skin friction coefficient upstream of, inside and downstream of grooves.

a clear restart at the downstream flat surface, while the large area of the groove smoothly absorbs some longitudinal momentum into the crisp recirculating flow and prevents it from interfering with the remainder of the main flow crossing over. This explains the relatively small jump in friction coefficient downstream of the groove in figure 4. From preliminary runs done for this study, the structure of the detachment/reattachment does not change much when the inter-groove spacing of 2 mm is increased. However, the reduction in the friction coefficient starts to decrease, as they become smaller than the large-scale longitudinal vortices. This agrees well with experimental drag characteristic measurements done by Ching et al. on a tow tank but for comparable Reynolds numbers [5].

Figure 3 shows a velocity vector plot of the middle triangular groove discussed earlier. One immediately notices the lower stagnation point inside the inclined backward facing side of the groove. The boundary layer developed therein grows longer in this case, disturbing further the main flow over the groove. Greater near-wall secondary flow motion contributes to drag increase, as is evident by previous plots and integrals. Additionally, even more clear in this figure are the two sizeable recirculation zones inside the groove. The two ensuing stagnation points give rise to the ensuing fluctuations in friction coefficient noticed in figure 4, and the horizontal components of these clearly contribute to the deteriorated performance of these grooves in this study.

For the case of semicircular grooves the stagnation point is also high, similar to the square groove case. Thus the spike in skin friction at the restart of the boundary layer is much lower than the triangular groove. The comfortable, monotonic development of the boundary layer inside the groove, however, adds to the skin friction cost of these grooves.

4 Conclusions and future work

In this paper, the turbulent flow over transversely grooved surfaces was numerically studied. Three different groove geometries were constructed and compared on the basis of reduction in total skin friction coefficient. Skin friction values and behavior inside the grooves was a good indicator of how the flow exiting them would disturb the main flow and to what degree. The optimum groove was one that succeeds in terminating the boundary layer but does not introduce high cross flow at the beginning of the next straight section of the surface. In general, square grooves outperformed comparable triangular and semi-circular grooves in the medium turbulent Reynolds number ranges. It was found that the dynamics of the flow inside the grooves, the nature of separation and reattachment of the flow, and the location of the stagnation point influenced what happens downstream of the grooves greatly. For the studied groove sizes and spacings, the results favor square grooves for the Reynolds number range reported herein. Higher Reynolds number simulations would shed more light on the dynamics of interaction between the flow inside the grooves and the main parallel flow but then compressibility effects must be considered, which are not the subject of this paper.

The results validate the notion that optimally grooved surfaces might greatly benefit efforts to reduce viscous drag which will increase the efficiency and enhance the performance of many engineering devices in numerous applications across the industry. Future work in this area is to optimize the shape of the groove as to accomplish the above goal. This might be in the form of using jigsaw-shaped surfaces in a way that achieves the desired detachment and reattachment effect for maximum drag reduction. Another possibility to use *deep* grooves or completely open slits in the surface to accomplish the desired effect. Further optimization of inter-groove spacing is required, and different ranges of Reynolds number must also be studied to develop a more complete picture. The effect of the turbulent boundary layer modification on Nusselt number is also interesting. The question of whether heat transfer enhancement must come at the expense of drag (increase) is an interesting one. It is equally interesting to explore the possibility of existence of a pure hydrodynamic technique that alleviates the dependence of shear stress of Reynolds number as suggested by Polidori et al. [10] using temperature difference.

One final note about the numerics is that the solution tends to stagnate short of convergence when using single precision due to the large order of magnitude difference between the various equations. Even for moderate Reynolds numbers, the non-scaled residuals of turbulent dissipation rate and continuity equations are 10 orders of magnitude apart. That said, the prospects of using CFD as a valid tool to investigate such flows and geometry, in the opinion of the authors, still outshine many of the current experimental techniques due to the large number of data points required for the necessary measurements and the large fluctuations in quantities near rough surfaces. Nevertheless, CFD simulations will never replace experimental work. Only validated numerical models can give insight to the underlying physical aspects of such flows. This stipulates undertaking a thorough comparison



between the results obtained here and the experimental work conducted by Ching and Parsons [5], which agree favorably thus far.

References

- [1] Hama, F.R., Long, J.D. & Hegarty, J.C., On transition from laminar to turbulent flow. *Journal of Applied Physics*, **28**(4), pp. 388–394, 1957.
- [2] Kline, S.J., Reynolds, W.C., Schraub, F.A. & Runstadler, P.W., The structure of turbulent boundary layers. *Journal of Fluid Mechanics*, **30**, pp. 741–773, 1967.
- [3] Viswanath, P.R., Aircraft viscous drag reduction using riblets. *Progress in Aerospace Sciences*, **38**, pp. 571–600, 2002.
- [4] Tani, I., Munakat, H., Matsumoto, A. & Abe, K., Turbulence management by groove roughness. *Turbulence Management and Relaminarization*, eds. H.W. Liepman & R. Narasimha, Springer-Verlag, pp. 161–172, 1987.
- [5] Ching, C.Y. & Parsons, B.L., Drag characteristics of turbulent boundary layer over a flat plate with transverse square grooves. *Experiments in Fluids*, **26**, pp. 273–275, 1999.
- [6] Caram, J.M. & Ahmed, A., Development on the wake of an airfoil with riblets. *AIAA Journal*, **30**(12), pp. 2817–2818, 1992.
- [7] Kramer, M.O., Boundary-layer stabilization by distributed damping. *Journal of the aeronautical sciences*, **24**, pp. 459–460, 1957.
- [8] Gad-el-Hak, M., Compliant coatings for drag reduction. *Progress in Aerospace Sciences*, **38**, pp. 77–99, 2002.
- [9] Katoh, K., Choi, K.S. & Azuma, T., Heat-transfer enhancement and pressure loss by surface roughness in turbulent channel flows. *International Journal of Heat and Mass Transfer*, **43**, pp. 4009–4017, 2000.
- [10] Polidori, G., Taiar, R., Fohanno, S., Mai, T.H. & Lodini, A., Skin-friction drag analysis from the forced convection modeling in simplified underwater swimming. *Journal of Biomechanics*, **39**(13), pp. 2535–2541, 2006.
- [11] Endo, T., Kasagi, N. & Suzuki, Y., Feedback control of wall turbulence with wall deformation. *International Journal of Heat and Fluid Flow*, **21**, pp. 568–575, 2000.
- [12] Wahidi, R., Chakroun, W. & Al-Fahed, S., The behavior of the skin-friction coefficient of a turbulent boundary layer flow over a flat plate with differently configured transverse square grooves. *Experimental Thermal and Fluid Science*, **30**(2), pp. 141–152, 2005.
- [13] Wilcox, D.C., *Turbulence Modelling for CFD*. DCW Industries Inc.: La Canada, CA, USA, 1993.
- [14] Fluent Inc., Lebanon, NH, USA, *FLUENT 6.2 User's Guide*, 2005.

